Forsch Ingenieurwes (2023) 87:697–710
https://doi.org/10.1007/s10010-023-00640-3

ORIGINALARBEITEN/ORIGINALS

Robust two-degrees of freedom linear quadratic gaussian position control for the front axle actuator of a steer-by-wire system

Robert Gonschorek[1] · **Torsten Bertram**[1]

Received: 2 July 2021 / Accepted: 21 January 2023 / Published online: 17 February 2023

Abstract
The Steer-by-Wire (SbW) system is a key technology for highly automated driving. For automated lateral vehicle guidance, the precise position control of the SbW Front Axle Actuator is an essential prerequisite. This contribution presents the modeling, control design, nominal performance, and stability analysis as well as the robustness analysis of the position control for the SbW Front Axle Actuator. Based on a nonlinear model of the plant a simplified linear system model is derived. This model yields the basis for the design of a Two-Degrees of Freedom Linear Quadratic Gaussian Control (2DOF LQG control), which allows an independent design of the command and the disturbance response. Besides an evaluation of the nominal control behavior, μ-analysis is applied to assess the robustness of performance and stability. Finally, real vehicle tests for different driving maneuvers are presented to verify simulation results.

Robuste Zwei-Freiheitsgrade Linear Quadratisch Gaußsche Positions-regelung für den Vorderachsaktuator eines Steer-by-Wire Systems

Zusammenfassung
Die Steer-by-Wire (SbW) Lenkung ist eine Schlüsseltechnologie für hochautomatisiertes Fahren. Für die automatisierte Fahrzeugquerführung ist dabei eine präzise Positionsregelung des SbW Vorderachsaktuators wesentliche Voraussetzung. Dieser Beitrag beschreibt die Modellbildung, Reglersynthese, Analyse der nominalen Regelgüte und Stabilität sowie die Robustheitsanalyse einer Positionsregelung für den SbW Vorderachsaktuator. Ausgehend von einem nichtlinearen Modell der Regelstrecke wird ein vereinfachtes lineares Systemmodell entwickelt. Dieses bildet die Grundlage für den Entwurf einer Zwei-Freiheitsgrade Linear Quadratisch Gaußschen Positionsregelung (2DOF LQG Regelung), welche es ermöglicht, das Führungs- und das Störverhalten unabhängig voneinander einzustellen. Neben der Evaluation der nominalen Regelgüte erfolgt eine μ-Analyse, um die Robustheit der Regelgüte und Stabilität zu bewerten. Abschließend werden reale Fahrversuche mit verschiedenen Fahrmanövern vorgestellt, um die Ergebnisse aus der Simulation zu verifizieren.

1 Introduction

Upcoming vehicle generations will provide fault-tolerant onboard power supply systems and an increasing level of driving automation. These changes contribute to the applicability of SbW systems, which are considered a key technology for highly automated driving [1]. For automated lateral vehicle guidance, the SbW Front Axle Actuator must provide accurate steering position tracking. Thereby, high requirements regarding dynamics, steady-state accuracy, and robustness must be fulfilled, which require an active compensation of rack forces and nonlinear friction. For meeting these requirements, a 2DOF LQG position control is proposed. This control concept allows an independent design of the command and the disturbance response of the control loop by combining a model-based dynamic feedforward control with an observer-based optimal state-feedback control. Moreover, by using all system states for the controller, a specific design of the complete system dynamics is achieved.

✉ Robert Gonschorek
robert.gonschorek@tu-dortmund.de

Torsten Bertram
torsten.bertram@tu-dortmund.de

[1] Institut für Roboterforschung, Technische Universität Dortmund, Dortmund, Germany

Most works in literature that treat the design of position controllers for Electric Power Steering systems (EPS) or Steer-by-Wire systems (SbW) base on a linear plant model with nominal parameters [2–5]. Classical stability margins such as gain and phase margin (GM, PM) are used to assess the robustness of the control system [4]. However, these margins indicate the robustness of stability to unstructured gain or phase variations, and it is not straightforward how they relate to physical quantities (e.g. parameter variation). In [6] individual plant parameters are varied, and the resulting Nyquist plots of the open-loop system are analyzed. Nevertheless, this involves the risk of missing critical parameter combinations, which lead to instability. The robustness of performance is often assessed in a similar way using nonlinear simulation analysis (see [13]). Therefore, robust performance cannot be guaranteed for all possible parameter combinations of the plant.

The control method employed for the SbW system must be robust to plant uncertainty. Conventional sliding mode control methods frequently face the problem of chattering issues [7]. Some improvements are proposed by different authors to handle this problem. In [8] an optimal integral sliding mode control is suggested to ensure low chattering, high bandwidth reference tracking and energy efficiency [9]. propose a super-twisting sliding mode control that guarantees robustness and mitigates the chattering effect. However, this approach increases the computational burden, which may exceed the controller sampling time. In [10] and [11] a Linear Quadratic Regulator (LQR) controller is proposed that is robust to parameter perturbations and is real time capable. However, specific numerical evidence on the robustness against plant parameter uncertainty is not given. Moreover, all of these works provide verification to the results purely in simulation or on a hardware in the loop test bench. However, both will differ significantly from the situation in a real road vehicle. The artificial test setup cannot cover the complexity of a real driving maneuver [12]. tested a variety of different operating conditions using synthetic excitation signals, such as sinusoidal and dual-shift line steering commands. However, the influence of different steering velocities and vehicle speeds on the SbW system has not been reflected.

This contribution describes the design of the position controller for the Front Axle Actuator of an SbW system. After modeling and analysis of the system plant, a 2DOF LQG position controller is systematically designed. The nominal control performance and stability are assessed using time and frequency domain analysis. Subsequently, a systematic approach for the quantitative assessment of robust performance and stability is adopted. For this purpose, the nominal control system is extended by uncertainty models and performance weighting functions, and an analysis of the structured singular value (μ-analysis) is conducted. The paper ends with a verification of simulation results using real vehicle tests. Hereby, different driving maneuvers and vehicle speeds are considered to get a representative view of the control performance.

2 Modeling and system analysis

Figure 1 shows the general structure of the SbW system. It consists of the Hand Wheel Actuator (HWA) for simulating the required force feedback to the driver and the Front Axle Actuator (FAA) for steering the road wheels according to the measured steering wheel angle. Furthermore, an electro-mechanical clutch is installed, which is disengaged during normal operation and engaged in failure mode only. The clutch serves as a mechanical fall back in case of a system failure. Some vehicle manufacturers have the stringent requirement that the SbW system must be equipped with a clutch as a mechanical fallback. The FAA comprises of a permanent magnet synchronous motor (1), which is connected via a worm gear (2) to the rack (3), a pinion shaft (4), a torsion bar (5), and the lower half of the clutch (6).

The torsion bar torque and lower steering angle are measured by sensors. For deriving a mathematical model, which accurately reflects the essential plant dynamics, the system components are modeled by spring, damper, mass, and gear elements (Fig. 2):

In this context, the electric motor inertia (J_{EM}) is rigidly coupled to the pinion inertia (J_{PN}) via the worm gear and rack and pinion gear. For model simplification, the rack mass is lumped to the pinion. The pinion inertia itself is coupled to the lower half of the clutch inertia (J_{CL}) by an elastic torsion bar. For modeling the elasticity of the torsion bar, a spring-damper element with linear stiffness (c_{TS}) and damping (d_{TS}) is used. The rotatory motion of the inertias is described by the state variables angular position (φ_i) and angular velocity ($_i$) regarding inertial reference frames.

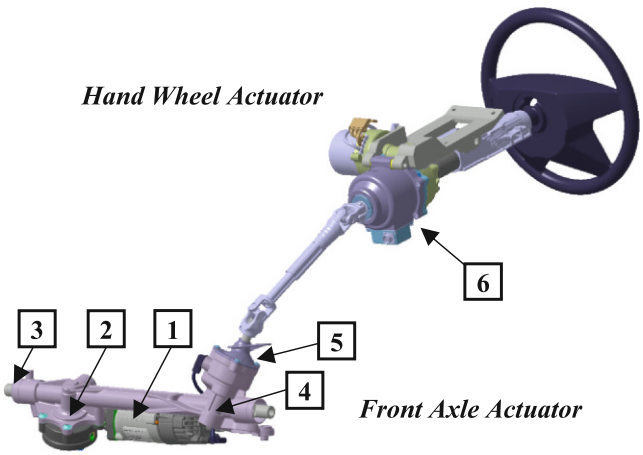

Fig. 1 Steer-by-Wire system

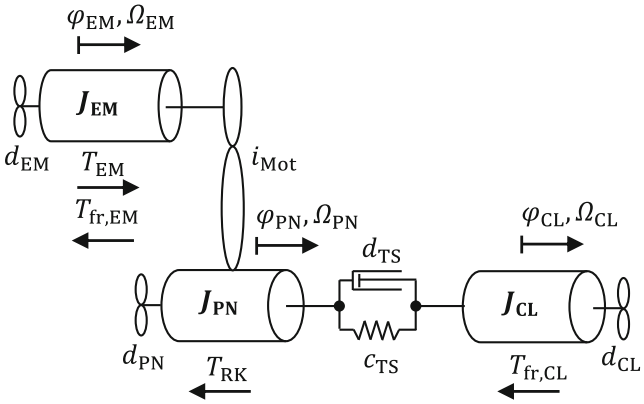

Fig. 2 Mechanical Model of the Front Axle Actuator

The mechanical system model is driven by the output torque of the electric motor (T_{EM}). The external load torque (T_{RK}) and nonlinear friction torques ($T_{fr,EM}, T_{fr,CL}$) act as disturbances. To consider viscous friction the inertias are augmented by linear damping elements (d_{EM}, d_{PN}, d_{CL}). By drawing the free-body diagrams of the inertias and deriving the equations of motion (Newton's law), the differential equations of the system are derived as [14]:

$$J_{EM}\dot{\Omega}_{EM} = T_{EM} - d_{EM}\Omega_{EM} - T_{fr,EM} - T_{React} \quad (1)$$
$$J_{PN}\dot{\Omega}_{PN} = T_{React}i_{Mot} + T_{TB} - d_{PN}\Omega_{PN} - T_{RK} \quad (2)$$
$$J_{CL}\dot{\Omega}_{CL} = -T_{TB} - d_{CL}\Omega_{CL} - T_{fr,CL} \quad (3)$$

With:

$$T_{TB} = c_{TS}(\varphi_{CL} - \varphi_{PN}) + d_{TS}(\Omega_{CL} - \Omega_{PN}) \quad (\varphi_{CL} > \varphi_{PN} \text{ and } \Omega_{CL} > \Omega_{PN}) \quad (4)$$

These are further simplified through the elimination of the internal reaction torques (T_{React}) in Eqs. 1 and 2. Moreover, the electric motor and pinion inertia are lumped to a substitute inertia ($J_{\overline{PN}}$), which yields:

$$J_{\overline{PN}}\dot{\Omega}_{PN} = T_{EM}i_{Mot} + T_{TB} - T_{fr,PN} - T_{RK} - d_{\overline{PN}}\Omega_{PN} \quad (5)$$
$$J_{CL}\dot{\Omega}_{CL} = -T_{TB} - d_{CL}\Omega_{CL} - T_{fr,CL} \quad (6)$$

With:

$$J_{\overline{PN}} = J_{PN} + i_{Mot}^2 J_{EM} \quad (7)$$
$$d_{\overline{PN}} = d_{PN} + i_{Mot}^2 d_{EM} \quad (8)$$
$$T_{fr,PN} = i_{Mot}T_{fr,EM} \quad (9)$$

The dynamics of motor current control are approximated by a first-order lag

$$\dot{T}_{EM} = -\omega_{bw}T_{EM} + \omega_{bw}T_{EM}^* \quad (10)$$

with ω_{bw} reflecting the actuator control bandwidth and T_{EM}^* the motor torque demand.

For deriving a linearized plant model from Eqs. 5 to 10, the nonlinear terms ($T_{RK}, T_{fr,PN}, T_{fr,CL}$) are dropped and treated as unknown disturbance inputs. Furthermore, the pinion position φ_{PN}, pinion velocity Ω_{PN}, difference position $\Delta\varphi = \varphi_{CL} - \varphi_{PN}$, difference velocity $\Delta\Omega = \Omega_{CL} - \Omega_{PN}$, and motor torque T_{EM} are selected as states. Thereby the equations can be transformed into the following state-space representation:

$$\dot{\underline{\mathbf{x}}}_{\boldsymbol{p}} = \underline{\mathbf{A}}_{\boldsymbol{p}}\underline{\mathbf{x}}_{\boldsymbol{p}} + \underline{\mathbf{B}}_{\boldsymbol{c},\boldsymbol{p}}u_{c,p} + \underline{\mathbf{B}}_{\boldsymbol{d},\boldsymbol{p}}\underline{\mathbf{u}}_{\boldsymbol{d},\boldsymbol{p}} \quad (11)$$

$$y_{o,p} = \underline{\mathbf{C}}_{\boldsymbol{o},\boldsymbol{p}}\underline{\mathbf{x}}_{\boldsymbol{p}}$$

$$\underline{\mathbf{y}}_{\boldsymbol{m},\boldsymbol{p}} = \underline{\mathbf{C}}_{\boldsymbol{m},\boldsymbol{p}}\underline{\mathbf{x}}_{\boldsymbol{p}}$$

with

$$\underline{\mathbf{A}}_{\boldsymbol{p}} = \begin{bmatrix} 0 & 1 & 0 & 0 & 0 \\ 0 & -\frac{d_{\overline{PN}}}{J_{\overline{PN}}} & \frac{c_{TS}}{J_{\overline{PN}}} & \frac{d_{TS}}{J_{\overline{PN}}} & \frac{i_{Mot}}{J_{\overline{PN}}} \\ 0 & 0 & 0 & 1 & 0 \\ 0 & -\frac{d_{CL}}{J_{CL}} + \frac{d_{\overline{PN}}}{J_{\overline{PN}}} & -\frac{c_{TS}}{J_{CL}} - \frac{c_{TS}}{J_{\overline{PN}}} & -\frac{d_{CL}+d_{TS}}{J_{CL}} - \frac{d_{TS}}{J_{\overline{PN}}} & -\frac{i_{Mot}}{J_{\overline{PN}}} \\ 0 & 0 & 0 & 0 & -\omega_{bw} \end{bmatrix}$$

$$\underline{\mathbf{B}}_{\boldsymbol{c},\boldsymbol{p}} = \begin{bmatrix} 0 \\ 0 \\ 0 \\ 0 \\ \omega_{bw} \end{bmatrix}, \underline{\mathbf{B}}_{\boldsymbol{d},\boldsymbol{p}} = \begin{bmatrix} 0 & 0 \\ -\frac{1}{J_{\overline{PN}}} & 0 \\ 0 & 0 \\ \frac{1}{J_{\overline{PN}}} & \frac{1}{J_{CL}} \\ 0 & 0 \end{bmatrix}, \underline{\mathbf{x}}_{\boldsymbol{p}} = \begin{bmatrix} \varphi_{PN} \\ \Omega_{PN} \\ \Delta\varphi \\ \Delta\Omega \\ T_{EM} \end{bmatrix},$$

$$\underline{\mathbf{C}}_{\boldsymbol{m},\boldsymbol{p}} = \begin{bmatrix} 1 & 0 & 0 & 0 & 0 \\ 0 & 0 & c_{TS} & 0 & 0 \end{bmatrix},$$

$$\underline{\mathbf{y}}_{\boldsymbol{m},\boldsymbol{p}} = \begin{bmatrix} \varphi_{PN} \\ T_{TS} \end{bmatrix}, u_{c,p} = \begin{bmatrix} T_{EM}^* \end{bmatrix},$$

$$\underline{\mathbf{C}}_{\boldsymbol{o},\boldsymbol{p}} = \begin{bmatrix} 1 & 0 & 0 & 0 & 0 \end{bmatrix}, \underline{\mathbf{u}}_{\boldsymbol{d},\boldsymbol{p}} = \begin{bmatrix} T_{fr,PN} + T_{RK} \\ T_{fr,CL} \end{bmatrix}. \quad (12)$$

The physical model parameters were determined experimentally through system identification. Figure 3 shows the system identification and model validation results. For controller design the relevant frequency range are frequencies up to the target bandwidth. Thereover, the disturbances in the position control system are typically low frequent (e.g. rack forces and friction). Therefore, a frequency range up to 30 Hz is reasonable and the high frequency behavior of the plant can be neglected. Performance assessment in the vehicle is done to confirm that this assumption is valid.

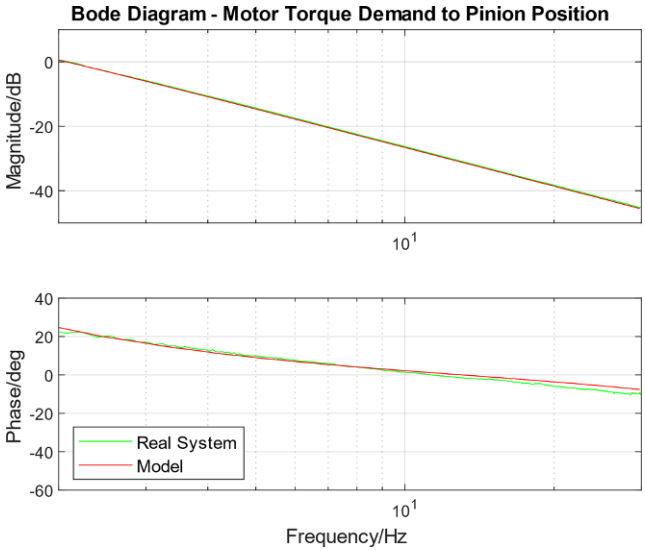

Fig. 3 Frequency Response of the Model and Real System

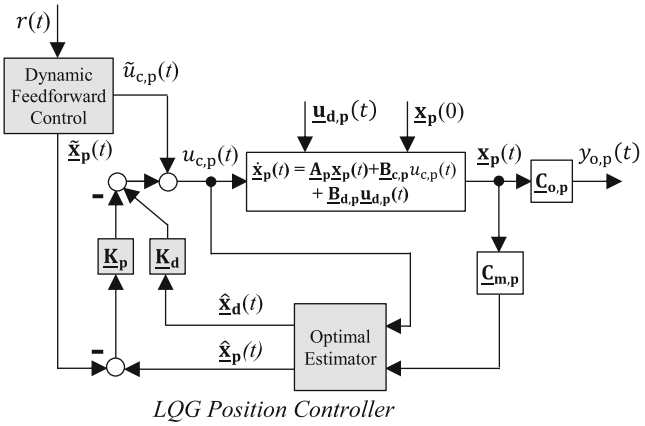

Fig. 4 Two-Degrees of Freedom LQG Position Control

For the system identification a sine sweep excitation signal with frequencies from 1 to 30 Hz was injected as the motor torque demand (plant control input) and the pinion position (controlled variable) was measured. From the recorded time signals the frequency response of the model and the real system was computed. The system identification results show a good correspondence between model and real system over the entire frequency range. Hence, it is ensured that the model accurately reflects the essential dynamics of the real system.

3 Design of a 2DOF LQG control

This section outlines the systematic design of a 2DOF LQG position control. The general control structure is illustrated in Fig. 4 and results from combining a model-based dynamic feedforward control with an LQG feedback control (i.e. combination of LQR controller and Kalman Filter). Here $r(t)$ represents the reference pinion position that is provided by the measured steering wheel angle in manual driving mode or by a lane guidance controller in automated driving mode. The signal $y_{o,p}$ reflects the pinion position and is the objective variable for control.

This has the advantage that the dynamics of the command and the disturbance response of the control system can be independently designed. Thereover, the entire system dynamics can be arbitrarily designed as the linear plant model is fully controllable and state-space control methods are applied [15, 16].

In the following section, the design of an LQG control is initially described, which defines the dynamics of the disturbance response and the stability. It consists of an optimal state-feedback control and an optimal state-estimator. Thereafter, a model-based dynamic feedforward control is introduced, which allows to specifically design the command response of the control loop. The connection of feedback control and dynamic feedforward control ultimately results in the 2DOF LQG position control.

3.1 Optimal state-feedback control

For the linear plant model with objective output equation

$$\dot{\underline{\mathbf{x}}}_{\boldsymbol{p}} = \underline{\mathbf{A}}_{\boldsymbol{p}}\underline{\mathbf{x}}_{\boldsymbol{p}} + \underline{\mathbf{B}}_{\boldsymbol{c},\boldsymbol{p}}u_{c,p} \qquad \text{with: } \underline{\mathbf{u}}_{\boldsymbol{d},\boldsymbol{p}} = \underline{\mathbf{0}} \tag{13}$$

$$y_{o,p} = \underline{\mathbf{C}}_{\boldsymbol{o},\boldsymbol{p}}\underline{\mathbf{x}}_{\boldsymbol{p}}$$

an optimal control $u_{c,p}$ is needed, which drives the state vector $\underline{\mathbf{x}}_{\boldsymbol{p}}$ from any initial state to the zero state, such that the value of a performance index is minimized. For the performance index, a quadratic cost function J_r build by the weighted control input and objective output is used

$$J_r = \int_0^\infty \left[y_{o,p}^T Q\, y_{o,p} + u_{c,p}^T R u_{c,p}\right] dt. \tag{14}$$

The weighting factors $Q \geq 0$ and $R > 0$ penalize large values of the respective signals in the minimization of the cost function. A simple and physically meaningful choice is to select Q and R as [14]:

$$Q = \frac{1}{\text{max.acceptable value of } y_{o,p}^2}$$

$$R = \frac{1}{\text{max.acceptable value of } u_{c,p}^2}$$

Following this rule, the variables that appear in the cost function J_r are scaled so that the maximum acceptable value of each term is 1. By application of this method, good starting values for the optimal controller design are obtained, which can be further refined by additional controller design and analysis iterations. The state-feedback

$$u_{c,p} = -\underline{\mathbf{K}}_{\boldsymbol{p}}\underline{\mathbf{x}}_{\boldsymbol{p}} \tag{15}$$

is the optimal control, which minimizes the quadratic cost function over an infinite time horizon $[0, \infty]$. The controller gain matrix $\underline{\mathbf{K}}_{\boldsymbol{p}}$ follows from [16]

$$\underline{\mathbf{K}}_{\boldsymbol{p}} = \underline{\mathbf{R}}^{-1}\underline{\mathbf{B}}_{c,p}^{T}\underline{\mathbf{S}} \tag{16}$$

where $\underline{\mathbf{S}}$ is the steady-state solution of the matrix Riccati equation

$$\underline{\mathbf{A}}_{\boldsymbol{p}}^{T}\underline{\mathbf{S}} + \underline{\mathbf{S}}\underline{\mathbf{A}}_{\boldsymbol{p}} - \underline{\mathbf{S}}\underline{\mathbf{B}}_{c,p}\underline{\mathbf{R}}^{-1}\underline{\mathbf{B}}_{c,p}^{T}\underline{\mathbf{S}} + \underline{\mathbf{C}}_{o,p}^{T}\underline{\mathbf{Q}}\underline{\mathbf{C}}_{o,p} = \underline{\mathbf{0}} \tag{17}$$

The optimal state-feedback control determines the dynamics of the disturbance response and the stability.

For steady-state disturbance rejection, a static disturbance feedforward is further added. The extended control law is

$$u_{c,p} = -\underline{\mathbf{K}}_{\boldsymbol{p}}\underline{\mathbf{x}}_{\boldsymbol{p}} + \underline{\mathbf{K}}_{\boldsymbol{d}}\underline{\mathbf{x}}_{\text{dist}} \tag{18}$$

and requires that the disturbance variables $\underline{\mathbf{x}}_{\text{dist}}$ can be measured or estimated. The gains $\underline{\mathbf{K}}_{\boldsymbol{d}}$ of the static disturbance feedforward can be analytically calculated for the linear plant model with objective output equation by [17]

$$\underline{\mathbf{K}}_{\boldsymbol{d}} = -\left[\underline{\boldsymbol{\phi}}\underline{\mathbf{B}}_{c,p}\right]^{-1}\underline{\boldsymbol{\phi}}\underline{\mathbf{B}}_{d,p} \quad \text{with } \underline{\boldsymbol{\phi}} = -\underline{\mathbf{C}}_{o,p}\left[\left(\underline{\mathbf{A}}_{\boldsymbol{p}} - \underline{\mathbf{B}}_{c,p}\underline{\mathbf{K}}_{\boldsymbol{p}}\right)\right]^{-1} \tag{19}$$

3.2 Optimal state-estimator

For optimal state-feedback controller design, it was supposed that the disturbance variables are available as measurements. However, this is not the case in practical implementation. Therefore, a state-estimator is designed, which provides estimates of the plant states and reconstructs the unknown disturbance variables.

For the design of the state-estimator, the linear plant model with measurement output equation

$$\begin{aligned}\dot{\underline{\mathbf{x}}}_{\boldsymbol{p}} &= \underline{\mathbf{A}}_{\boldsymbol{p}}\underline{\mathbf{x}}_{\boldsymbol{p}} + \underline{\mathbf{B}}_{c,p}u_{c,p} + \underline{\mathbf{B}}_{\boldsymbol{d},p}\underline{\mathbf{u}}_{\boldsymbol{d},p}\\ \underline{\mathbf{y}}_{\boldsymbol{m},p} &= \underline{\mathbf{C}}_{\boldsymbol{m},p}\underline{\mathbf{x}}_{\boldsymbol{p}}\end{aligned} \tag{20}$$

is augmented by unknown input integrator disturbance models

$$\begin{aligned}\dot{\underline{\mathbf{x}}}_{\text{dist}} &= \underline{\mathbf{A}}_{\text{dist}}\underline{\mathbf{x}}_{\text{dist}} + \underline{\mathbf{B}}_{\text{dist}}\underline{\mathbf{u}}_{\text{dist}}\\ \underline{\mathbf{y}}_{\text{dist}} &= \underline{\mathbf{C}}_{\text{dist}}\underline{\mathbf{x}}_{\text{dist}}\end{aligned} \quad \text{with : } \underline{\mathbf{A}}_{\text{dist}} = \underline{\mathbf{0}}, \underline{\mathbf{B}}_{\text{dist}} = \underline{\mathbf{I}}, \underline{\mathbf{C}}_{\text{dist}} = \underline{\mathbf{I}}. \tag{21}$$

Using the substitution $\underline{\mathbf{u}}_{\boldsymbol{d},\boldsymbol{p}} = \underline{\mathbf{y}}_{\text{dist}}$ the extended linear plant model results [14, 16]

$$\begin{bmatrix}\dot{\underline{\mathbf{x}}}_{\boldsymbol{p}}\\ \dot{\underline{\mathbf{x}}}_{\text{dist}}\end{bmatrix} = \begin{bmatrix}\underline{\mathbf{A}}_{\boldsymbol{p}} & \underline{\mathbf{B}}_{\boldsymbol{d},\boldsymbol{p}}\underline{\mathbf{C}}_{\text{dist}}\\ \underline{\mathbf{0}} & \underline{\mathbf{A}}_{\text{dist}}\end{bmatrix}\begin{bmatrix}\underline{\mathbf{x}}_{\boldsymbol{p}}\\ \underline{\mathbf{x}}_{\text{dist}}\end{bmatrix} + \begin{bmatrix}\underline{\mathbf{B}}_{c,p} & \underline{\mathbf{0}}\\ \underline{\mathbf{0}} & \underline{\mathbf{B}}_{\text{dist}}\end{bmatrix}\begin{bmatrix}u_{c,p}\\ \underline{\mathbf{u}}_{\text{dist}}\end{bmatrix}$$

$$\underline{\mathbf{y}}_{\boldsymbol{m},\boldsymbol{p}} = \begin{bmatrix}\underline{\mathbf{C}}_{\boldsymbol{m},\boldsymbol{p}} & \underline{\mathbf{0}}\end{bmatrix}\begin{bmatrix}\underline{\mathbf{x}}_{\boldsymbol{p}}\\ \underline{\mathbf{x}}_{\text{dist}}\end{bmatrix} \tag{22}$$

respectively in compact matrix-/vector notation

$$\begin{aligned}\dot{\underline{\mathbf{x}}}_{\boldsymbol{a}} &= \underline{\mathbf{A}}_{\boldsymbol{a}}\underline{\mathbf{x}}_{\boldsymbol{a}} + \underline{\mathbf{B}}_{\boldsymbol{a}}\underline{\mathbf{u}}_{\boldsymbol{a}}\\ \underline{\mathbf{y}}_{\boldsymbol{a}} &= \underline{\mathbf{C}}_{\boldsymbol{a}}\underline{\mathbf{x}}_{\boldsymbol{a}}\end{aligned} \tag{23}$$

Based on the augmented linear plant model, an optimal state-estimator (Kalman filter) is designed. For the optimal estimation problem, it is assumed that the augmented plant is disturbed by process noise $\underline{\mathbf{w}}$ and measurement noise $\underline{\mathbf{v}}$. In this context, the process noise is modeled additive to the inputs for penalizing the unknown disturbance model inputs and preparing for input Loop Transfer Recovery (LTR). The latter is a Kalman filter adjustment procedure that asymptotically recovers the excellent robustness properties for full-state feedback and thereby contributes to the robust design of the LQG control [14, 16, 19, 20].

For the augmented plant model subject to process and measurement noise an optimal state estimate $\hat{\underline{\mathbf{x}}}_{\boldsymbol{a}}(t)$ is needed, which minimizes the steady-state value of the sum of the squared estimation errors

$$J_e = \lim_{t\to\infty} \text{sp}\left[\text{E}\left\{\left(\underline{\mathbf{x}}_{\boldsymbol{a}} - \hat{\underline{\mathbf{x}}}_{\boldsymbol{a}}\right)\left(\underline{\mathbf{x}}_{\boldsymbol{a}} - \hat{\underline{\mathbf{x}}}_{\boldsymbol{a}}\right)^{T}\right\}\right] = \lim_{t\to\infty} \text{sp}\left[\underline{\mathbf{P}}_{\boldsymbol{e}}\right] \tag{24}$$

The optimal solution is given by the state-estimator

$$\dot{\hat{\underline{\mathbf{x}}}}_{\boldsymbol{a}} = \left(\underline{\mathbf{A}}_{\boldsymbol{a}} - \underline{\mathbf{L}}\underline{\mathbf{C}}_{\boldsymbol{a}}\right)\hat{\underline{\mathbf{x}}}_{\boldsymbol{a}} + \underline{\mathbf{B}}_{\boldsymbol{a}}\underline{\mathbf{u}}_{\boldsymbol{a}} + \underline{\mathbf{L}}\underline{\mathbf{y}}_{\boldsymbol{a}} \tag{25}$$

that minimizes the quadratic cost function over the infinite time horizon $[0, \infty]$. The state-estimator feedback gain matrix $\underline{\mathbf{L}}$ is computed from [16]

$$\underline{\mathbf{L}} = \underline{\mathbf{P}}_{\boldsymbol{e}}^{*}\underline{\mathbf{C}}_{\boldsymbol{a}}^{\boldsymbol{T}}\underline{\mathbf{V}}^{-1} \tag{26}$$

with $\underline{\mathbf{P}}_{\boldsymbol{e}}^{*}$ the steady-state solution of the Riccati equation

$$\underline{\mathbf{A}}_{\boldsymbol{a}}\underline{\mathbf{P}}_{\boldsymbol{e}}^{*} + \underline{\mathbf{P}}_{\boldsymbol{e}}^{*}\underline{\mathbf{A}}_{\boldsymbol{a}}^{\boldsymbol{T}} - \underline{\mathbf{P}}_{\boldsymbol{e}}^{*}\underline{\mathbf{C}}_{\boldsymbol{a}}^{\boldsymbol{T}}\underline{\mathbf{V}}^{-1}\underline{\mathbf{C}}_{\boldsymbol{a}}\underline{\mathbf{P}}_{\boldsymbol{e}}^{*} + \underline{\mathbf{B}}_{\boldsymbol{a}}\underline{\mathbf{W}}\underline{\mathbf{B}}_{\boldsymbol{a}}^{\boldsymbol{T}} = \underline{\mathbf{0}} \tag{27}$$

The weighting matrices $\underline{\mathbf{W}}$ and $\underline{\mathbf{V}}$ can be treated as design parameters for the determination of the estimator feedback gain $\underline{\mathbf{L}}$. By assuming that the noise processes are uncorrelated, they become diagonal matrices whose elements are the variances of the respective noise vector components. Suitable starting values for the noise variances may be obtained by considering the environment of the estimator in the digital implementation. The control inputs will be fixed point values with a defined quantization that is given by the software scaling. The measurement outputs will also be subject to quantization, which is due to the limited resolution in the AD conversion of these signals. The resulting round-off errors can be modeled as stochastic white noise processes that are added to the respective signals. According to [14] the variance of quantization noise can be defined as:

$$\sigma^2 = \frac{q^2}{12}$$

with q being the signal quantization. Noise that does not originate from signal quantization, such as for example sensor noise, can be measured by experiment and the determined variance value used as a direct design parameter. By applying this rule to the control input and measurement output signals, suitable estimator design parameters can be found. All that remains is finding appropriate values for the noise variance of the integrator disturbance model inputs. As these inputs are unknown, their noise variances must be selected as high as possible (i.e. high uncertainty) to make the estimator fully rely on the measurements for their reconstruction. Summarizing these guidelines, physically meaningful initial values for the weighting matrices $\underline{\mathbf{W}}$ and $\underline{\mathbf{V}}$ are obtained by selecting:

$$W_{ii} = \text{variance of}\, u_{a,i}\,(k) \quad i \in \{1,2,...,l\}$$

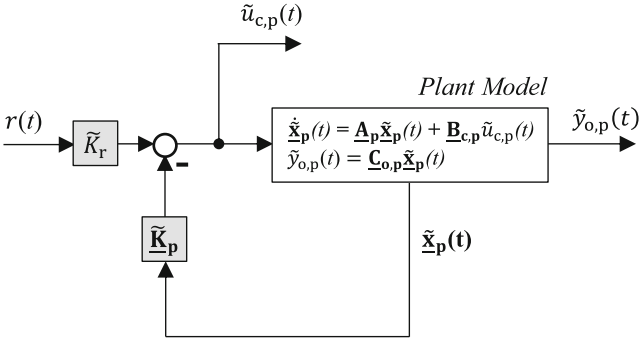

Fig. 5 Model-based Dynamic Feedforward Control

$$V_{jj} = \text{variance of}\, y_{a,i}\,(k) \quad j \in \{1,2,...,k\}$$

with

- the noise variance from quantization error computed by $\sigma^2 = q^2/12$
- the noise variance from sensor noise identified by experiment
- the noise variance for integrator disturbance model inputs selected as high as possible

The estimated state and disturbance variables are provided as input to the control law. By incorporating the integrator disturbance models into the state-estimator, the resulting LQG controller has integral action and is robust against plant uncertainty.

3.3 Model-based dynamic feedforward control

The LQG control defines the dynamics of the disturbance response and the stability of the closed-loop system. For an independent design of the dynamics of the command response, the model-based dynamic feedforward control is introduced (see Fig. 5). It consists of a virtual control loop, which is executed online to generate a control signal $\widetilde{u}_{c,p}$ for command following. The generated control signal is then provided to the real plant. For hiding the effect of the control signal on the system states from the LQG feedback controller, the virtual state vector $\widetilde{\underline{\mathbf{x}}}_{\boldsymbol{p}}$ is subtracted from the state estimates $\widehat{\underline{\mathbf{x}}}_{\boldsymbol{p}}$ (see Fig. 4).

Thereby, the LQG feedback controller accepts any intervention from dynamic feedforward control and remains inactive [15].

The virtual control loop is designed for the desired command response. For this purpose, the synthesis of an optimal state-feedback controller with static reference feedforward

is suitable as the state vector of the plant model is directly accessible [18]. The control law is

$$\widetilde{u}_{c,p} = -\widetilde{\underline{\mathbf{K}}}_{\boldsymbol{p}}\widetilde{\underline{\mathbf{x}}}_{\boldsymbol{p}} + \widetilde{K}_r r. \tag{28}$$

The optimal feedback gain matrix $\widetilde{\underline{\mathbf{K}}}_{\boldsymbol{p}}$ is analogous to Sect. 3.1 designed by minimization of a quadratic cost function. The static reference feedforward is analytically computed by [16]

$$\widetilde{\mathrm{K}}_r = -\left[\underline{\mathbf{C}}_{o,p}\left[\left(\underline{\mathbf{A}}_{\boldsymbol{p}} - \underline{\mathbf{B}}_{c,p}\widetilde{\underline{\mathbf{K}}}_{\boldsymbol{p}}\right)\right]^{-1}\underline{\mathbf{B}}_{c,p}\right]^{-1} \tag{29}$$

As the dynamic reference feedforward is a pure feedforward control, it has no impact on the stability of the control loop.

3.4 Two-degrees of freedom LQG control

By combining the model-based dynamic feedforward control with the LQG feedback control, the 2DOF LQG position control according to Fig. 4 results. For the absence of model error, disturbances, or different initial conditions the command response of the virtual control loop propagates to the real system. The LQG feedback controller remains inactive in this case. However, if different initial conditions, external disturbances, or model error occur, the LQG feedback controller becomes active and determines the disturbance response. Hence, the 2DOF control structure allows for a separate design of the command and the disturbance response of the control system [15, 17].

4 Nominal performance and stability analysis

After the control design, the nominal performance and stability of the 2DOF LQG position control are analyzed. For this purpose, time and frequency domain analysis of the linear control system is conducted. Figure 6 shows the step responses of the steering position for reference and disturbance excitation. To provide a performance comparison, the results are shown for the 2DOF LQG control and the conventional LQG control.

For a reference steering position step of 90°, the 2DOF LQG control achieves a rise time of 17 ms, an overshoot of 3.8%, and a settling time of 45 ms. In contrast, the conventional LQG control shows a rise time of 34 ms, an overshoot of 4.4% and a settling time of 97 ms. The injection of a disturbance step at pinion and at clutch reveals identical results for the 2DOF LQG control and LQG control. This is because the model-based dynamic feedforward con-

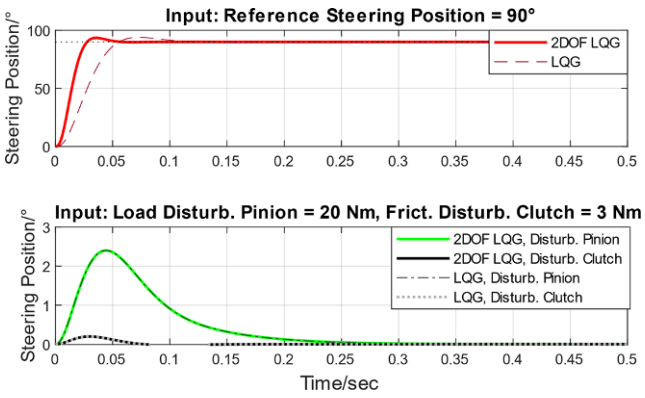

Fig. 6 Step Responses for Reference/Disturbance Excitation (simulation)

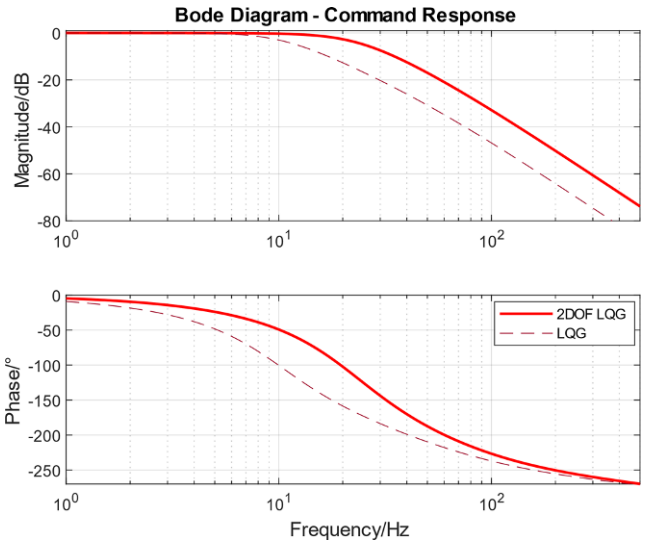

Fig. 7 Frequency Response for Command Following (simulation)

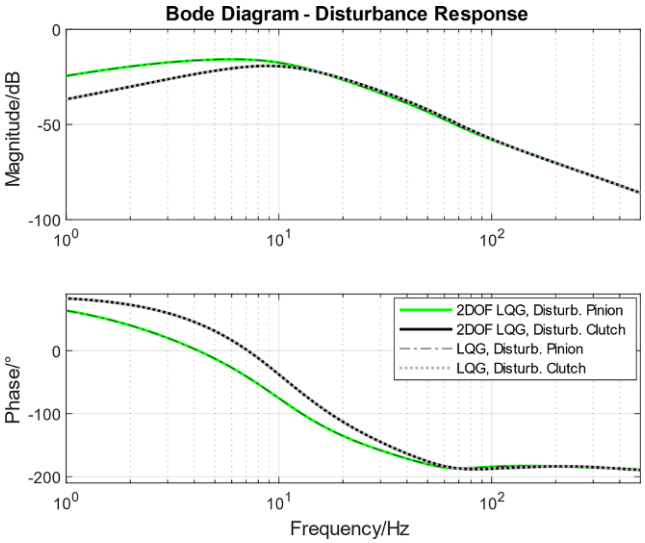

Fig. 8 Frequency Responses for Disturbance Rejection (simulation)

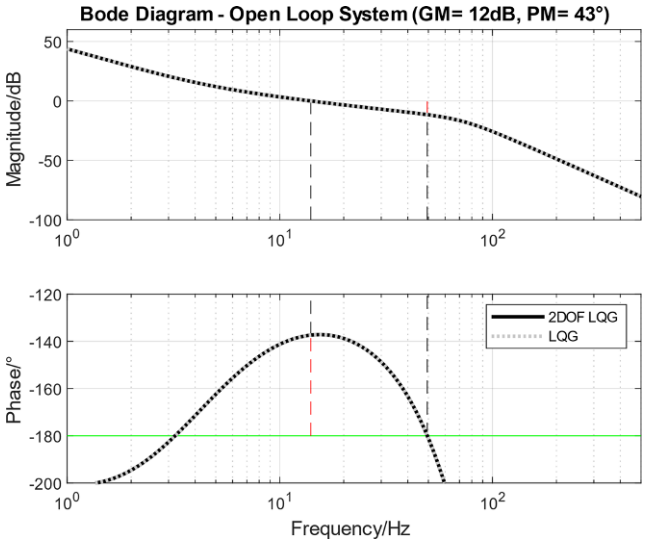

Fig. 9 Frequency Response of the Open Loop System (simulation)

trol only affects the command response of the control loop and the disturbance response remains unchanged. A load torque disturbance step of 20 Nm at pinion shows a maximum steering position error of 2.4°, which is eliminated within 200 ms. Similarly, a friction torque disturbance step of 3 Nm at clutch reveals a maxi-mum position error of 0.2°, which vanishes after 150 ms. Therefore, the designed control achieves a dynamic command following and is robust against unknown disturbances. In addition to the time responses, the frequency responses of the closed-loop system and open loop system are inspected (see Figs. 7, 8 and 9).

With this regard, the designed 2DOF LQG position control achieves a reference tracking bandwidth (i.e. magnitude drop by –3 dB) of 21 Hz. The conventional LQG control shows a reference tracking bandwidth of 10 Hz. Thereby, the advantages of the 2DOF control structure are exposed, which allows increasing the reference tracking bandwidth without degrading stability. This is because the model-based dynamic feedforward control is used for increasing the tracking bandwidth without changing the open loop transfer function (refer to Fig. 9). For a conventional 1DOF control structure, this is not possible (see [15]). Furthermore, the frequency responses from the plant disturbance inputs to the measured steering position are analyzed, which reflects the disturbance rejection of the control loop (see Fig. 8). Disturbance torques at pinion are attenuated by at least –15.8 dB and disturbance torques at clutch by at least –19.2 dB. Thereover steady-state disturbance rejection for both transfer paths is achieved.

Figure 9 depicts the frequency responses of the open-loop system that give the basis for stability analysis. They are identical for the 2DOF LQG control and conventional LQG control. The control loop has nominal stability and is robust to gain and phase variations, which is exposed by a gain margin of 12 dB and a phase margin of 43°. Under consideration of the good fit between the plant model and system (refer to Sect. 2), these margins can be considered satisfactory for covering plant parameter variations and neglected plant dynamics that may occur in practice.

For a more detailed analysis of the influence of plant parameter uncertainties and dynamic uncertainties on the stability and performance of the control system, a robustness analysis is presented next. In regard to robust disturbance rejection, we focus on rack force disturbances in the following, which are particularly critical for accurate position tracking.

5 Robustness analysis

In the previous section, the nominal stability and performance of the designed control were assessed. Robustness analysis is now conducted to evaluate if stability and performance are guaranteed in the presence of parametric and dynamic plant uncertainty. For this purpose, uncertainty models are defined in the following. Subsequently, performance weighting functions are designed that specify performance requirements in the frequency domain. The uncertainty models and performance weighting functions are then added to the nominal control system to get the uncertain control system. By introducing virtual inputs and outputs, the uncertainty variables are extracted and collected in a perturbation matrix $\underline{\mathbf{\Delta}}$, and the remaining part of the system is converted into a transfer function matrix $\underline{\mathbf{N}}$. This $\underline{\mathbf{N}}$, $\underline{\mathbf{\Delta}}$-structure provides the foundation for robust stability and performance analysis using the structured singular value μ.

5.1 Modeling of uncertainties

For the modeling of plant uncertainties, parametric and dynamic uncertainties are considered. Parametric uncertainty is the deviation of a physical parameter from its nominal value and can be mathematically modeled as [19]:

$$p = \overline{p}\left(1 + \eta_p \delta_p\right), \delta_p \rightarrow \mathbb{R}, \quad -1 \leq \delta_p \leq 1 \tag{30}$$

with

$\overline{p}$ nominal parameter value,
η_p uncertainty weight,
δ_p normalized uncertainty variable

With this respect the following parametric uncertainties are considered for the linearized plant model (Table 1).

Furthermore, a dynamic multiplicative input uncertainty is assumed to account for simplifications in the actuator

Table 1 Parametric Uncertainties

p	$\overline{p}$	η_p	δ_p
J_{CL}	$\overline{J}_{\mathrm{CL}} = 0.001\ \mathrm{kg}m^2$	$\eta_{J_{\mathrm{CL}}} = 0.15$	$\lvert\delta_{J_{\mathrm{CL}}}\rvert \leq 1$
$J_{\overline{\mathrm{PN}}}$	$\overline{J}_{\overline{\mathrm{PN}}} = 0.116\ \mathrm{kg}m^2$	$\eta_{J_{\overline{\mathrm{PN}}}} = 0.15$	$\lvert\delta_{J_{\overline{\mathrm{PN}}}}\rvert \leq 1$
d_{CL}	$\overline{d}_{\mathrm{CL}} = 0.05$ Nms/rad	$\eta_{d_{\mathrm{CL}}} = 0.5$	$\lvert\delta_{d_{\mathrm{CL}}}\rvert \leq 1$
$d_{\overline{\mathrm{PN}}}$	$\overline{d}_{\overline{\mathrm{PN}}} = 0.68$ Nms/rad	$\eta_{d_{\overline{\mathrm{PN}}}} = 0.5$	$\lvert\delta_{d_{\overline{\mathrm{PN}}}}\rvert \leq 1$
c_{TS}	$\overline{c}_{\mathrm{TS}} = 183.4$ Nm/rad	$\eta_{c_{\mathrm{TS}}} = 0.05$	$\lvert\delta_{c_{\mathrm{TS}}}\rvert \leq 1$

modeling, and neglected high-frequency dynamics of the plant. The dynamic uncertainty is modeled as [19]:

$$G = \overline{G}\,(1 + W_A \Delta_A)\,,\ \Delta_A \epsilon \mathbb{C},\ \ \|\Delta_A\|_\infty \leq 1 \tag{31}$$

with

$\overline{G}(s)$ nominal actuator transfer function,
$W_{\mathrm{A}}(s)$ uncertainty weight transfer function (fixed),
$\Delta_{\mathrm{A}}(s)$ normalized uncertainty transfer function (variable)

The uncertainty weight is frequency-dependent and modeled by a lead-lag filter

$$W_A\,(s) = \frac{s+a}{\frac{1}{K_u}s + \frac{1}{K_l}a}, a = 2\pi f_c \sqrt{\frac{\left(1 - 1/K_u^2\right)}{\left(1/K_l^2 - 1\right)}} \tag{32}$$

with $K_l = 0.05$ and $K_u = 1.5$ for a 5% gain uncertainty at low frequencies and 150% gain uncertainty at high frequencies. The gain cross-over is selected in line with the actuator bandwidth to $f_c = 50\,\mathrm{Hz}$.

5.2 Modeling of performance requirements

For robust performance analysis, weighting functions $W_{\mathrm{i}}(s)$ are defined in the frequency domain. These weighting functions specify upper bounds on the command response and the disturbance response of the uncertain control system [19]. With this regard, the performance requirements for the command response are modeled by a second-order lag filter

$$W_1^{-1}\,(s) = \frac{K_{\mathrm{dc}}}{\frac{1}{\omega_0^2}s^2 + \frac{\sqrt{2}}{\omega_0}s + 1} \tag{33}$$

with

$K_{\mathrm{dc}} = 1.1$
$\omega_0 = 2\pi\, f_0,\ f_0 = 30\,\mathrm{Hz}$

as shown in Fig. 10. Thus, the requirements are that the maximum gain must not exceed 0.83 dB (abs 1.1). Moreover, a maximum cut-off frequency of 30 Hz and a high-frequency gain roll off-of at least –40 dB/dec is required to ensure acceptable measurement noise attenuation and avoid the excitation of unmodeled high-frequency dynamics. The performance requirements for the disturbance response are modeled by a lead-lag filter

$$W_2^{-1}(s) = \frac{s+a}{\frac{1}{K_u}s + \frac{1}{K_l}a} \tag{34}$$

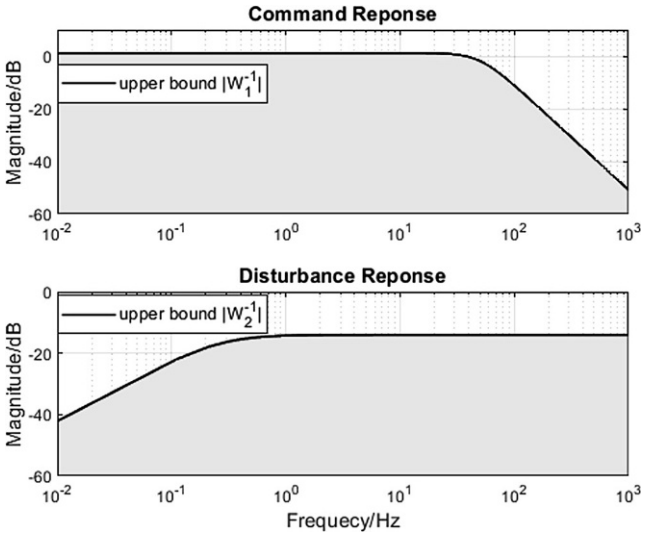

Fig. 10 Performance Requirements Specification

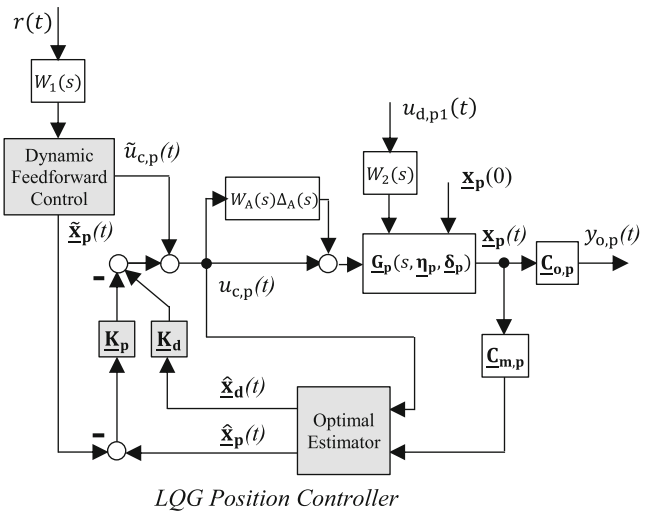

Fig. 11 Uncertain Control Loop with Performance Weights

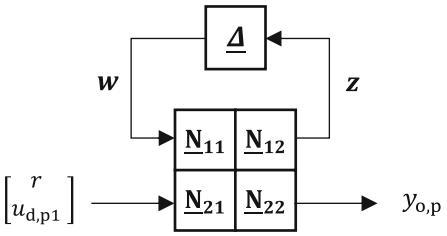

Fig. 12 $\underline{\mathbf{N}}$, $\underline{\mathbf{\Delta}}$ —LFR of the Uncertain Control Loop

with

$K_u = 0.2,\ K_l = 0.0001,$
$a = 0.0008$

Therefore, it is required that the minimum disturbance attenuation is –14 dB (abs 0.2) over the entire frequency range, which provides a strong rejection of external load torques. Furthermore, a steady-state disturbance attenuation of at least –80 dB (abs 0.0001) is required to ensure stationary accuracy of the position control.

5.3 Augmentation of the nominal control system

The previously defined parametric uncertainties, dynamic uncertainty, and performance weighting functions are now added to the nominal control system. For this purpose, the nominal physical parameters are replaced by uncertain physical parameters in the state-space equations of the plant model. Furthermore, the dynamic uncertainty is inserted at the plant control input. Finally, the performance weighting functions are connected to the reference and the disturbance input. This gives the uncertain control loop with performance weighting as shown in Fig. 11.

To get a suitable format for μ-analysis, the uncertain control loop must be transformed into a Linear Fractional Representation (LFR). This is accomplished by introducing virtual inputs w and outputs z, which allow a separation of the unknown uncertainty variables δ_i, Δ_i.

The separated uncertainty variables are collected in a perturbation matrix $\underline{\mathbf{\Delta}}$(s). The remaining "known part" of the system can be transformed into a transfer function matrix $\underline{\mathbf{N}}$(s) that is connected to $\underline{\mathbf{\Delta}}$(s) in a feedback configuration. Thereby, the $\underline{\mathbf{N}}$, $\underline{\mathbf{\Delta}}$—LFR of the uncertain control loop shown in Fig. 12 is obtained, which gives the foundation for robust stability and performance analysis [19].

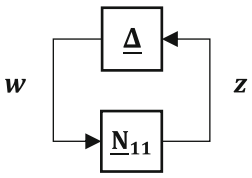

Fig. 13 LFR setup for Robust Stability Analysis

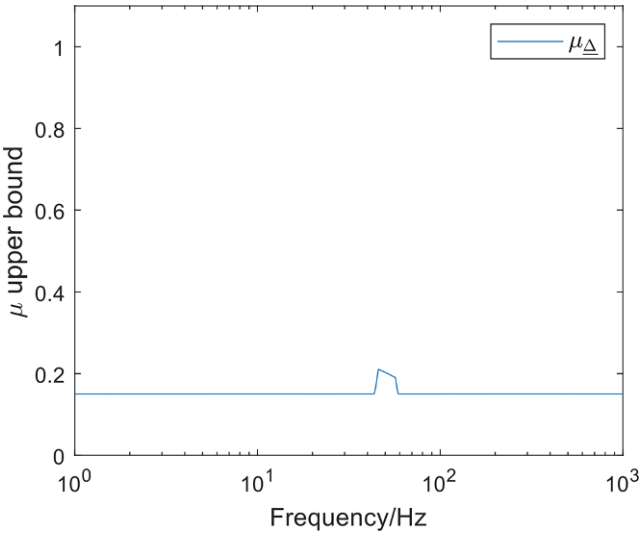

Fig. 14 $\mu_{\underline{\mathbf{\Delta}}}$ upper bound for robust stability

Partitioning of $\underline{\mathbf{N}}$ and merging it with $\underline{\mathbf{\Delta}}$ gives the transfer function matrix $\underline{\mathbf{F}}$ of the uncertain control loop:

$$\underline{\mathbf{F}} = \underline{\mathbf{N}}_{22} + \underline{\mathbf{N}}_{21}\underline{\mathbf{\Delta}}\left(\mathbf{I} - \underline{\mathbf{N}}_{11}\underline{\mathbf{\Delta}}\right)^{-1}\underline{\mathbf{N}}_{12}$$

$$y_{o,p} = \underline{\mathbf{F}} \cdot \begin{bmatrix} r \\ u_{d,p1} \end{bmatrix} \tag{35}$$

5.4 Robust stability analysis

For analyzing robust stability, only the elements $\underline{\mathbf{N}}_{11}$ are needed, which are connected to the perturbation matrix $\underline{\mathbf{\Delta}}$ in a feedback configuration, that is (Fig. 13).

The structured singular value ($\mu_{\underline{\mathbf{\Delta}}}$) is introduced to formulate necessary and sufficient conditions for robust stability. The mathematical definition is given as:

$$\begin{aligned} \mu_{\underline{\mathbf{\Delta}}}{}^{-1} &= \min\left\{\bar{\sigma}\left(\underline{\mathbf{\Delta}}\right) \left|\det\left(\mathbf{I} - \underline{\mathbf{N}}_{11}\underline{\mathbf{\Delta}}\left(j\omega\right)\right) = 0\right.\right\} \\ \mu_{\underline{\mathbf{\Delta}}} &= 0, \quad \text{if no such structured } \underline{\mathbf{\Delta}} \text{ exists} \end{aligned} \tag{36}$$

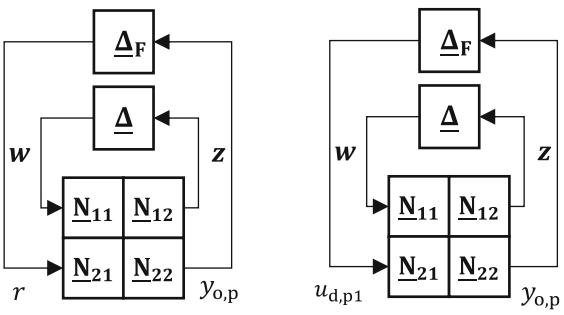

Fig. 15 LFR setup for Robust Performance Analysis of the command and disturbance response

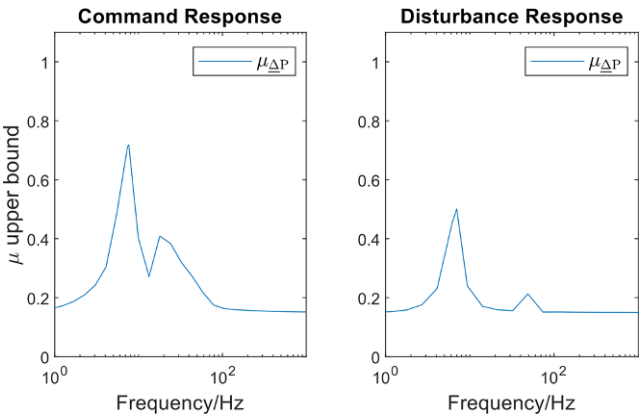

Fig. 16 $\mu_{\underline{\Delta}_P}$ upper bounds for robust performance

Therefore, $\mu_{\underline{\Delta}}$ is defined as the reciprocal value of the smallest perturbation $\underline{\Delta}$ (measured by $\bar{\sigma}(\underline{\Delta})$), for which $\det\left(\underline{\mathbf{I}} - \underline{\mathbf{N}}_{11}\underline{\Delta}(j\omega)\right)$ becomes 0 and thus instability occurs. Hence, the system is robustly stable if and only if $\mu_{\underline{\Delta}} < 1$ for all frequencies [19].

Figure 14 shows the computed $\mu_{\underline{\Delta}}$ upper bound over frequency, which provides a numerical approximation to the exact $\mu_{\underline{\Delta}}$ value. The peak value of the upper bound is 0.21. Therefore, the control system is robustly stable for the modeled uncertainty. It can tolerate up to 474% of the considered uncertainty before instability occurs.

Hence, the peak value of $\mu_{\underline{\Delta}}$ provides a quantitative measure for the robustness of the 2DOF LQG position control system.

5.5 Robust performance analysis

For analyzing robust performance, the entire transfer function matrix $\underline{\mathbf{N}}$ is needed, and a fictitious complex uncertainty $\underline{\Delta}_F$ connecting the reference input and the objective output respectively the disturbance input and the objective output is introduced (Fig. 15).

Thus, the robust performance analysis can be transformed into a robust stability analysis problem [19]. The structured singular value $\mu_{\underline{\Delta}_P}$ for the augmented perturbation matrix

$$\underline{\Delta}_P = \begin{bmatrix} \underline{\Delta}_F & \underline{0} \\ \underline{0} & \underline{\Delta} \end{bmatrix}$$

and the matrix $\underline{\mathbf{N}}$ is introduced to formulate necessary and sufficient conditions for robust performance. The mathematical definition for $\mu_{\underline{\Delta}_P}$ is given by:

$$\begin{aligned} \mu_{\underline{\Delta}_P}{}^{-1} &= \min\left\{\bar{\sigma}\left(\underline{\Delta}_P\right) | \det\left(\underline{\mathbf{I}} - \underline{\mathbf{N}}\underline{\Delta}_P\left(\mathrm{j}\omega\right)\right) = 0\right\} \\ \mu_{\underline{\Delta}_P} &= 0, \text{ if no such structured } \underline{\Delta}_P \text{ exists} \end{aligned} \tag{37}$$

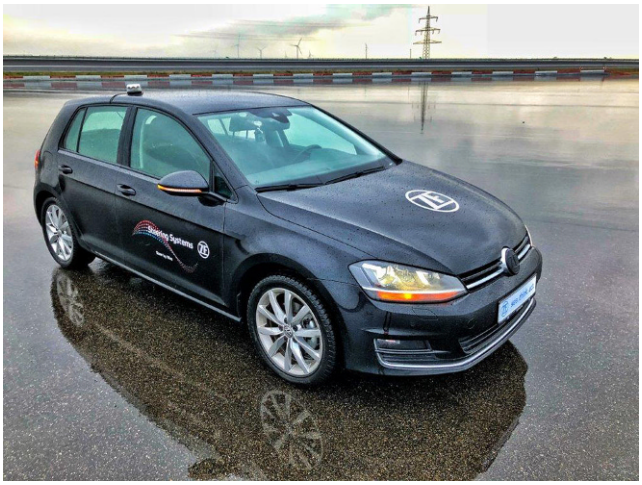

Fig. 17 Steer-by-Wire VW Golf 7 prototype vehicle

Table 2 Driving Maneuvers for Vehicle Performance Evaluation

Driving Maneuver	Vehicle Speed
Step steering	30, 60 and 100 kph
Sweep steering	30, 60 and 100 kph
Slalom	30, 40 and 50 kph

Therefore, the designed controller achieves robust performance if $\mu_{\underline{\Delta}_P} < 1$ for all frequencies [19].

Figure 16 illustrates the $\mu_{\underline{\Delta}_P}$ upper bounds over frequency for the command response and the disturbance response control performance. The peak value of the upper bound of $\mu_{\underline{\Delta}_P}$ for the command response is 0.72. Therefore, the control system has robust performance and fulfills the performance requirements for all of the modeled uncertainty. The uncertainty can be increased by up to 139% before requirements are violated. Similarly, by computing the upper bound of $\mu_{\underline{\Delta}_P}$ for the disturbance response, a peak value of 0.5 is found, thereby proving robust performance. The control system can tolerate up to 200% of the modeled uncertainty before performance requirements are no longer met.

For a robust stability and robust performance evaluation based on μ-analysis for the Front Axle Actuator position control, to the authors best knowledge, no data for a comparison was published.

6 Vehicle performance evaluation

After the assessment of robust stability and robust performance, real vehicle tests for different driving maneuvers are conducted to verify simulation results. With this regard the control performance is extensively tested for large reference steering angles, nonlinear disturbances (e.g. external rack forces, nonlinear friction), signal quantization, mea-

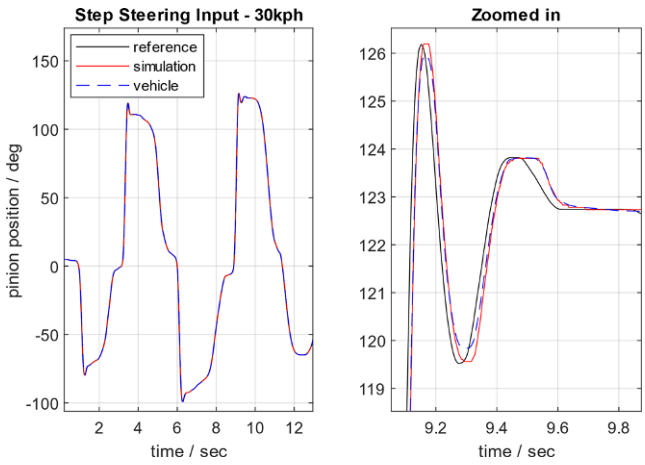

Fig. 18 Step Steering at 30 kph—Simulation vs. Vehicle

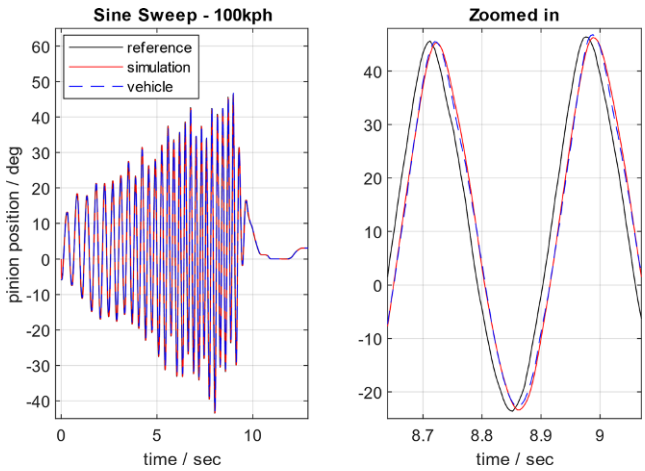

Fig. 19 Sweep Steering at 100 kph—Simulation vs. Vehicle

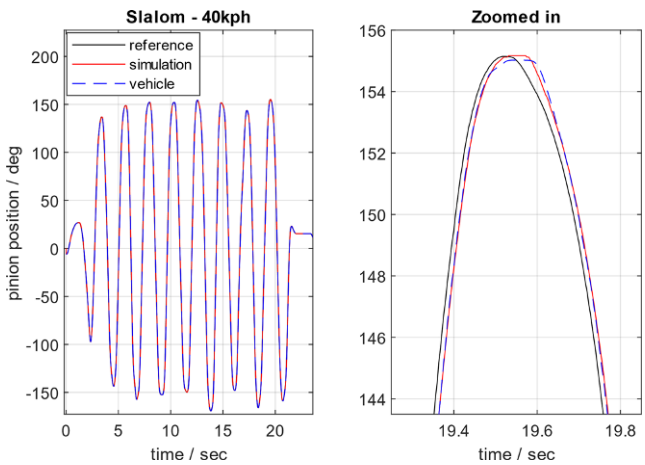

Fig. 20 Slalom at 40 kph—Simulation vs. Vehicle

surement noise, sampling effects and parameter variation/uncertainty. The test vehicle is a VW Golf 7 equipped with a SbW system as shown in Fig. 17.

The developed 2DOF LQG position control is auto-coded, compiled, and flashed on the microcontroller of the FAA system for direct embedded testing. Table 2 provides an overview on the different driving maneuvers, which were performed for vehicle speeds up to 100 kph.

The time signals from real vehicle tests (i.e. reference steering position, load torque, vehicle speed) are recorded and used as an input to nonlinear simulation analysis. Thereby, a direct comparison between simulated model outputs and real vehicle measurements can be conducted to confirm the validity of simulation results. For the simulation environment a MATLAB/Simulink model of the nonlinear differential equations of the system plant is used.

6.1 Vehicle results vs. nonlinear simulation

The controller design was fine-tuned iteratively in the vehicle together with a professional test driver compromising performance, robustness, NVH, and steering feel. Thereby an optimal setting was identified and used as the basis for all driving maneuvers presented in the following. Figure 18, 19 and 20 exemplarily show the control performance in the real vehicle against nonlinear simulation for step steering at 30 kph, sweep steering at 100 kph, and slalom at 40 kph. The step and sweep response driving maneuver are carried out to test the dynamic vehicle response and the command following of the position control.

The controller dynamically tracks the reference steering position with minor phase delay given by the control bandwidth. Disturbances originating from external rack forces, nonlinear friction or plant parameter uncertainty are strongly rejected and compensated in steady state. Moreover, the controller showed a stable behavior over the complete operating range of the system in all driving maneuvers. Thereby the robustness of the designed control in practical application is confirmed. Besides the performance evaluation, Fig. 18 to 19 reveal a good fit between the vehicle results and simulation, thereby providing verification to the simulation results. Figure 20 shows the results of a slalom driving maneuver at 40 kph.

The controller accurately follows the given reference profile and robustly rejects unknown disturbances. Again, an accurate fit between vehicle and simulation was achieved, which verifies the validity of the nonlinear simulation. Minor deviations during motion reversals are observable, which are due to the difficultly of modeling nonlinear friction.

Additional tests for parking conditions were performed using artificially generated reference step and sine sweep excitation signals. Hereby, the control performance was ex-

tensively tested for high load and high steering velocity conditions. In all of the tests performed, a good correspondence between vehicle measurement and simulation was achieved.

7 Conclusions

In this contribution, a nonlinear model of the Front Axle Actuator for a SbW system was derived and linearized. System identification and model validation confirmed a good fit between model and real system. A 2DOF LQG position control was synthesized, which allows an independent design of the command and the disturbance response of the control system. Thus, the reference tracking bandwidth of the position control can be increased without degrading the stability of the control system. The 2DOF LQG controller design was followed by a μ-analysis to quantitatively assess the robustness of performance and stability. Thereby, an iterative controller design and analysis process was employed to determine a controller, which fulfills the stability and performance requirements for the defined structured and unstructured plant uncertainties. Finally, the nonlinear simulation results were verified using real vehicle tests. Hereby, different driving maneuvers and vehicle speeds were considered to detailly test the control performance. The control fulfills the high requirements for automated driving and is robust against plant uncertainty. Furthermore, its modular structure proved itself as particularly useful for the tuning work in the prototype vehicle.

8 Appendix

Table 3 Variable Description

J_{EM}	Electric motor inertia	$u_{c,p}$	Control input
J_{PN}	Pinion inertia	$\underline{\mathbf{u}}_{\boldsymbol{d},\boldsymbol{p}}$	Disturbance inputs
J_{CL}	Clutch inertia (lower)	$\underline{\mathbf{x}}_{\boldsymbol{p}}$	State vector—plant
i_{Mot}	Gear ratio	$y_{o,p}$	Objective output
$J_{\overline{\mathrm{PN}}}$	Substitute inertia	$\underline{\mathbf{y}}_{\boldsymbol{m},\boldsymbol{p}}$	Measurement outputs
T_{TB}	Torsion bar torque	$\underline{\mathbf{A}}_{\boldsymbol{p}}$	System matrix
c_{TS}	Torque sensor stiffness	$\underline{\mathbf{B}}_{\boldsymbol{c},\boldsymbol{p}}$	Control input matrix
d_{TS}	Torque sensor damping	$\underline{\mathbf{B}}_{\boldsymbol{d},\boldsymbol{p}}$	Disturb. input matrix
φ_i	Angular position	$\underline{\mathbf{C}}_{\boldsymbol{o},\boldsymbol{p}}$	Object. output matrix
Ω_i	Angular velocity	$\underline{\mathbf{C}}_{\boldsymbol{m},\boldsymbol{p}}$	Meas. output matrix
$\Delta\varphi$	Difference position	$\underline{\mathbf{u}}_{\mathrm{dist}}$	Dist. model inputs
$\Delta\Omega$	Difference velocity	$\underline{\mathbf{x}}_{\mathrm{dist}}$	Dist. model states
T^*_{EM}	Motor torque demand	$\underline{\mathbf{y}}_{\mathrm{dist}}$	Dist. model outputs
T_{EM}	Motor output torque	$\underline{\mathbf{A}}_{\mathrm{dist}}$	Dist. System Matrix
T_{RK}	Rack torque	$\underline{\mathbf{B}}_{\mathrm{dist}}$	Dist. Input Matrix
$T_{\mathrm{fr,EM}}$	Friction torque—motor	$\underline{\mathbf{C}}_{\mathrm{dist}}$	Dist. Output Matrix
$T_{\mathrm{fr,PN}}$	Friction torque—pinion	$\underline{\mathbf{K}}_{\boldsymbol{p}}$	State-feedback matrix
$T_{\mathrm{fr,CL}}$	Friction torque—clutch	$\underline{\mathbf{K}}_{\boldsymbol{d}}$	Static dist. feedforward
T_{React}	Reaction torque	$\widetilde{\underline{\mathbf{K}}}_{\boldsymbol{p}}$	Virt. feedback matrix
d_{EM}	Viscous friction—motor	$\widetilde{\mathrm{K}}_r$	Static ref. feedforward
d_{PN}	Viscous friction—pinion	Q, R	Lqr weighting factors
d_{CL}	Viscous friction—clutch	$\underline{\mathbf{v}}$	Measurement noise
$d_{\overline{\mathrm{PN}}}$	Substitute viscous frict	$\underline{\mathbf{w}}$	Process noise
ω_{bw}	Motor bandwidth	$\underline{\mathbf{L}}$	Estimator Matrix

Funding Open Access funding enabled and organized by Projekt DEAL.

Conflict of interest R. Gonschorek and T. Bertram declare that they have no competing interests.

References

1. Ewald V, Konigorski U (2019) Regelung eines redundant aktuierten Steer-by-Wire-Systems. Forsch Ingenieurwes 83(2):129–135
2. Govender V, Müller S (2016) Modelling and position control of an electric power steering system. IFAC 49(11):312–318
3. Xiong L, Jiang Y, Fu Z (2018) Steering angle control of autonomous vehicles based on active disturbance rejection control. IFAC 51(31):796–800
4. Govender V, Ortmann L, Müller S (2017) Synthesis and validation of a rack position controller for an electric power steering. IFAC 50(2):253–258
5. Zhang H, Zhao W (2018) Two-way H∞ control method with a fault-tolerant module for steer-by-wire system. Proc Inst Mech Eng Part C J Mech Eng Sci 232(1):42–56
6. Irmer M, Henrichfreise H (2020) Design of a robust LQG compensator for an electric power steering. IFAC 53(2):6624–6630
7. Castillo I, Freidovich LB (2020) Describing-function-based analysis to tune parameters of chattering reducing approximations of sliding mode controllers. Control Eng Pract 95:1–12
8. Norsahperi NMH, Danapalasingam KA (2020) An improved optimal integral sliding mode control for uncertain robotic manipulators with reduced tracking error, chattering, and energy consumption. Mech Syst Signal Process. https://doi.org/10.1016/j.ymssp.2020.106747
9. Sun Z, Zheng J, Man Z, Fu M, Lu R (2019) Nested adaptive super-twisting sliding mode control design for a vehicle steer-by-wire system. Mech Syst Signal Process 122:658–672
10. Zhang G, Wang X, Li L, Shao W (2021) Design and applications of steering angle tracking control with robust compensator for steer-by-wire system of intelligent vehicle. IFAC PapersOnLine 54(10):221–227
11. Zhang H, Zhao W (2017) Stability control strategy of steer-by-wire system based on LQG/LTR. Sci Chin Technol Sci 6:844–853
12. Zou S, Zhao W (2020) Synchronization and stability control of dual-motor intelligent steer-by-wire vehicle. Mech Syst Signal Process. https://doi.org/10.1016/j.ymssp.2020.106925
13. Govender V, Khazardi G, Weiskircher T, Keppler D, Müller S (2016) A PID and state space approach for the position control of an electric power steering. In: Bargende M, Reuss HC, Wiedemann J (eds) 16. Internationales Stuttgarter Symposium. Proceedings. Springer, Wiesbaden
14. Franklin GF, Powell JD, Emami-Naeini A (2019) Feedback control of dynamic systems. Pearson Prentice Hall, New Jersey
15. Lohmann B (2014) Entwurf im Zustandsraum – alle Systemgrößen einbeziehen. In: Skolaut W (ed) Maschinenbau. Springer, Heidelberg
16. Föllinger O (2016) Regelungstechnik – Einführung in die Methoden und ihre Anwendung. VDE, Berlin
17. Roppenecker G (2009) Zustandsregelung linearer Systeme – Eine Neubetrachtung. Automatisierungstechnik 57(10):491–498
18. Deutscher J (2012) Zustandsregelung verteilt-parametrischer Systeme. Springer, Heidelberg
19. Skogestad S, Postlethwaite I (2005) Multivariable feedback control: analysis and design. John Wiley, Chichester
20. Brunton SL, Kutz JN (2019) Data-driven science and engineering—machine learning, dynamical systems, and control. Cambridge University Press, Washington